High-Contrast PET of Melanoma Using ^{18}F-MEL050, a Selective Probe for Melanin with Predominantly Renal Clearance

Delphine Denoyer[1], Ivan Greguric[2], Peter Roselt[1], Oliver C. Neels[1], Nicolas Aide[1], Stephen R. Taylor[2], Andrew Katsifis[2], Donna S. Dorow[1], and Rodney J. Hicks[1,3]

[1]Centre for Molecular Imaging and Translational Research Laboratory, Peter MacCallum Cancer Centre, Melbourne, Victoria, Australia; [2]Radiopharmaceuticals Research Institute, Australian Nuclear Science and Technology Organisation, Menai, New South Wales, Australia; and [3]Department of Medicine, University of Melbourne, Melbourne, Victoria, Australia

The aim of this study was to evaluate the novel probe ^{18}F-6-fluoro-*N*-[2-(diethylamino)ethyl] pyridine-3-carboxamide (^{18}F-MEL050) for the imaging of primary and metastatic melanoma. **Methods:** PET using ^{18}F-MEL050 was performed in murine models of melanoma. The specificity of ^{18}F-MEL050 was studied by comparing its accumulation in pigmented B16-F0 allograft tumors with that of human amelanotic A375 xenografts using PET and high-resolution autoradiography. ^{18}F-MEL050 PET results were compared with ^{18}F-FDG PET, the current standard in melanoma molecular imaging. To test the ability of ^{18}F-MEL050 to assess the metastatic spread of melanoma, a murine model of lung metastasis was imaged by PET/CT, and results correlated with physical assessment of tumor burden in the lungs. **Results:** In pigmented B16-F0 grafts, ^{18}F-MEL050 PET yielded a tumor-to-background ratio of approximately 20:1 at 1 h and greater than 50:1 at 2 and 3 h. In the B16-F0 melanoma allograft model, tumor-to-background ratio was more than 9-fold higher for ^{18}F-MEL050 than for ^{18}F-FDG (50.9 ± 6.9 vs. 5.8 ± 0.5). No uptake was observed in the amelanotic melanoma xenografts. Intense uptake of ^{18}F-MEL050 was evident in metastatic lesions in the lungs of B16-BL6 tumor–bearing mice on PET at 2 h after tracer injection, with high concordance between ^{18}F-MEL050 accumulation on PET/CT and tumor burden determined at necroscopy. **Conclusion:** ^{18}F-MEL050 has a rapid tumor uptake and high retention with specificity for melanin, suggesting great potential for noninvasive clinical evaluation of suspected metastatic melanoma.

Key Words: melanoma imaging; small-animal PET; PET/CT; high-resolution autoradiography; fluoronicotinamide analogue

J Nucl Med 2010; 51:441–447
DOI: 10.2967/jnumed.109.070060

Preclinical imaging of murine models of melanoma using a novel probe, ^{18}F-6-fluoro-*N*-[2-(diethylamino)ethyl] pyridine-3-carboxamide (^{18}F-MEL050), provides high contrast due to melanin binding and rapid renal clearance, suggesting great potential for imaging of suspected metastatic melanoma.

Received Sep. 1, 2009; revision accepted Dec. 8, 2009.
For correspondence or reprints contact: Rodney Hicks, Centre for Molecular Imaging and Translational Research Laboratory, Peter MacCallum Cancer Centre, 12 St. Andrew's Place, East Melbourne, Victoria 3002, Australia. E-mail: Rod.Hicks@petermac.org
COPYRIGHT © 2010 by the Society of Nuclear Medicine, Inc.

Melanoma is a highly malignant tumor that originates in melanocytes. If not detected and resected at an early stage, it spreads rapidly to other tissues, including lymph nodes, lung, liver, and brain (*1*). Melanoma incidence and disease-related mortality have increased progressively in recent decades, making this disease a significant public health problem worldwide. Five-year survival is only 15% when widespread metastatic deposits are present but rises to 99% if the disease is detected before it has spread (*2*). Despite the development of new therapeutic agents and improvement of existing therapies, surgical excision remains the most effective treatment (*3*). Therefore, early detection of metastatic spread and accurate staging are of great importance in planning therapeutic intervention to improve patient outcome. In particular, there are a few patients with a limited number of sites of metastatic spread who may benefit from surgical resection (*4*).

Currently, ^{18}F-FDG PET is routinely used for the staging of melanoma and is particularly useful in the diagnosis of advanced disease, notably for the detection of visceral, deep soft-tissue and lymph node metastases (*5*). However, ^{18}F-FDG PET has a poor sensitivity for the initial assessment of early-stage malignant melanoma (*6,7*). Indeed, lesions of less than 1 cm are often missed by ^{18}F-FDG PET. Moreover, because the mechanism of uptake and cellular retention of ^{18}F-FDG involves increased glucose metabolism, which may also be seen in many other tumor types and in inflammatory conditions, this tracer lacks specificity for melanoma (*8,9*). Thus, more sensitive and specific tracers are urgently needed to increase the effectiveness of PET for early detection in melanoma.

In recent years, several other radiolabeled imaging probes have been evaluated for melanoma imaging, including methylene blue dye (*10*), monoclonal antibodies against melanoma-associated antigens (*11,12*), iodoamphetamine (*13*), α-melanocyte–stimulating hormone ana-

logs (*14,15*), and benzamide (BZA)-based compounds (*16,17*). To date, iodinated BZA analogs have been among the most promising of the newer melanoma radiotracers for both diagnosis and therapeutic applications.

Clinical trials have shown the usefulness of ^{123}I-*N*-(2-diethylaminoethyl)-4-iodobenzamide (^{123}I-BZA), ^{123}I-*N*-(diethylaminoethyl)-2-iodobenzamide (^{123}I-BZA$_2$), and ^{123}I-iodobenzamide to image cutaneous and ocular melanoma deposits with high specificity and sensitivity (*18–21*). More recently, a preclinical imaging study by our group demonstrated that a novel iodobenzylpiperazine, ^{123}I-MEL037, had rapid and 3-fold higher tumor uptake than ^{123}I-BZA$_2$, suggesting a potential for both melanoma imaging and therapeutic applications (*22*). A preliminary study also reported the synthesis and biodistribution of a PET radiopharmaceutical, *N*-(2-diethylaminoethyl)-4-^{18}F-fluorobenzamide (FBZA), showing great promise for PET (*23*). However, the overall promise of these compounds has been compromised by significant hepatobiliary clearance. This potentially limits detection of abdominal disease, particularly small-bowel metastases, and increases the possibility of nontarget tissue damage if longer-lived isotopes were used in a therapeutic setting. Therefore, the development of radiotracers with improved pharmacokinetic properties adapted specifically for melanoma imaging by PET and therapy remains an important goal. In particular, primarily renal excretion would be advantageous.

Previously, we reported the synthesis and radiochemical properties of a series of fluoronicotinamide compounds designed specifically for labeling with ^{18}F for melanoma imaging with PET. The most promising of these compounds, MEL050, had excellent tumor uptake, radiochemical stability, and pharmacokinetic properties, with predominant renal excretion (*24*). These positive characteristics suggest that ^{18}F-MEL050 should be a superior agent for PET of melanoma. The aim of the current study was to evaluate the melanoma imaging potential of ^{18}F-MEL050 using PET and high-resolution autoradiography in murine models of primary and metastatic melanoma.

MATERIALS AND METHODS

Cell Lines

B16-F0 and B16-BL6 murine melanotic melanoma cell lines were maintained in Dulbecco's modified Eagle's medium supplemented with 10% fetal calf serum, 2 mM L-glutamine, and 1 mM pyruvate. A375, a human amelanotic melanoma cell line, was cultured in RPMI supplemented with 10% fetal calf serum and 2 mM L-glutamine.

Animal Experiments

For subcutaneous tumor grafts, female C57BL/6 mice were inoculated on the right flank with 10^6 B16-F0 cells in 100 μL of Ca^{++}/Mg^{++}-free phosphate-buffered saline (PBS), and 10^6 A375 cells in 50 μL of 1:1 phosphate-buffered saline/Matrigel (BD Biosciences) were inoculated into BALB/c nude mice. Mice were imaged once tumor graft volumes had reached approximately 100 mm^3. For the lung metastasis model, 3×10^5 B16-BL6 cells in 100 μL of Ca^{++}/Mg^{++}-free phosphate-buffered saline were injected into the lateral tail vein of BALB/c nude mice that were imaged 15 d after inoculation.

Radiopharmaceuticals

^{18}F-FDG was purchased from Cyclotek Pty Ltd. MEL050 was labeled in an in-house radiochemistry facility according to the method recently described by our group (*24*). In short, ^{18}F-MEL050 was prepared by a 1-step radiosynthesis of no-carrier-added K-^{18}F-F-Kryptofix 222 (dimethylformamide [Merck], 150°C, 5 min), followed by high-performance liquid chromatography purification. Synthesis time was 60 min, with an end-of-synthesis yield of 35%−40%, radiochemical purity greater than 99%, and specific activity of 150–220 GBq/μmol. The final product was stable (>98%) in saline over 3 h.

Small-Animal PET of Melanoma Grafts

The mice were injected via the lateral tail vein with either 20–30 MBq of ^{18}F-MEL050 in 100 μL of saline or 12–18 MBq of ^{18}F-FDG in 100–200 μL of saline. For ^{18}F-FDG PET, mice were kept fasting for 3 h and anesthetized by inhalation of 2.5% isoflurane/50% O_2 in air delivered at a flow rate of 200 mL/min before the injection of tracer. Anesthesia was maintained for 20 min after injection to reduce background muscle and brown fat uptake of ^{18}F-FDG. At either 60, 120, or 180 min after ^{18}F-MEL050 injection and at 90 min after ^{18}F-FDG injection, animals were anesthetized in the same manner as described above and scanned on a Mosaic small-animal PET device (Philips). The resolution of this system was 2.7 mm at the center of the field of view (FOV) (*25*). The energy window was 450–700 keV, and the coincidence-timing window was 6 ns. Data were acquired in 3-dimensional mode and corrected for decay and randoms. Acquisition time was 10 min per bed position. Reconstruction was performed with the 3-dimensional RAMLA algorithm (*26,27*). Scatter and attenuation corrections were not applied.

To calculate tumor-to-background ratios (TBR), a region of interest (ROI) was drawn around the tumor, and a background region was chosen to represent the mediastinal blood pool excluding regions of tracer accumulation such as spleen. The maximum pixel value within the tumor ROI was then divided by the average pixel value within the background ROI. The percentage of injected dose per gram of tissue (%ID/g) was determined by dividing the %ID obtained for a given organ ROI by the weight of the lesion, assuming a density of 1 g/cm^3.

^{18}F-MEL050 PET/CT of Lung Metastasis Model

Four mice were imaged simultaneously on a human PET/CT device (Biograph 64 TrueV; Siemens Medical Solutions). For this experiment, 2 mice were placed at +2.5- and −2.5-cm radial offsets, and 2 were placed at +6.5- and −6.5-cm radial offsets from the center of the FOV.

The CT scan was acquired first, with the following parameters: 80 mAs; 130 kV; pitch, 1; and collimation, 64 × 0.6 mm. The CT image was reconstructed with a B60 kernel filter. Then, a PET static emission image was acquired in 3-dimensional mode for 10 min. PET images were reconstructed with a zoom of 2 (FOV, 35 cm) using a high-definition reconstruction algorithm that modeled point-spread function (TrueX; Siemens Medical Solutions) to achieve resolution recovery with a 2.2-mm spatial resolution at the center of the FOV. The following parameters were used: 6 iterations, 16 subsets, and matrix size equal to 336^2,

resulting in a 1.02 × 1.02 × 1 mm voxel size. Scatter and attenuation corrections were applied.

High-Resolution Autoradiography

Tumor-bearing mice were injected intravenously with 25–30 MBq of ^{18}F-MEL050. After 60 min, mice were sacrificed, and the tissues were removed, embedded in optimum-cutting-temperature medium (Tissue Tek), and snap-frozen in cooled isopentane. Frozen sections (20 μm) were cut on a cryostat at −12°C and thaw-mounted on glass microscope slides. After the sections were air-dried, they were covered with solid scintillation paper and scanned in a high-resolution autoradiographic imager (β-Micro-Imager; Biospace Lab). Disintegrations were recorded during a period of 2 h. Anatomic images of the scanned sections were recorded with a digital camera.

RESULTS

Whole-Body ^{18}F-MEL050 Small-Animal PET in B16-F0 Allografts

The chemical structure of ^{18}F-MEL050 is shown in Figure 1A. To first assess the overall imaging potential of this compound, C57BL/6 mice were implanted with B16-F0 nonmetastatic melanoma allografts and the mice imaged by ^{18}F-MEL050 PET when tumor volumes were above 100 mm^3. To determine the optimum time for tumor uptake, tumor-bearing mice were imaged at 1, 2, and 3 h after tail vein injection of 20–30 MBq of ^{18}F-MEL050 (Fig. 1B). The images revealed excellent tumor retention, with a low signal in nontarget tissues that enabled clear delineation of the tumor as early as 1 h after tracer injection. In a cohort of 6 mice, TBRs (Table 1) reached an average of 19.3 ± 1.9 at 1 h, rose to 50.9 ± 6.9 at 2 h, and remained at 54.3 ± 10.5 through the 3-h time point. The high level of radioactivity in the bladder at 1 h reduced significantly by 3 h, confirming that ^{18}F-MEL050 was rapidly and primarily excreted through the urinary system as previously reported (*24*). In the C57BL/6 mice, accumulation of the tracer in the eyes and spleen and a much-reduced level in the thyroid were also observed, whereas no uptake was observed in bone or other organs. Blocking the thyroid by giving mice drinking water supplemented with Lugol's solution for 3 d before ^{18}F-MEL050 PET failed to inhibit thyroid uptake (data not shown).

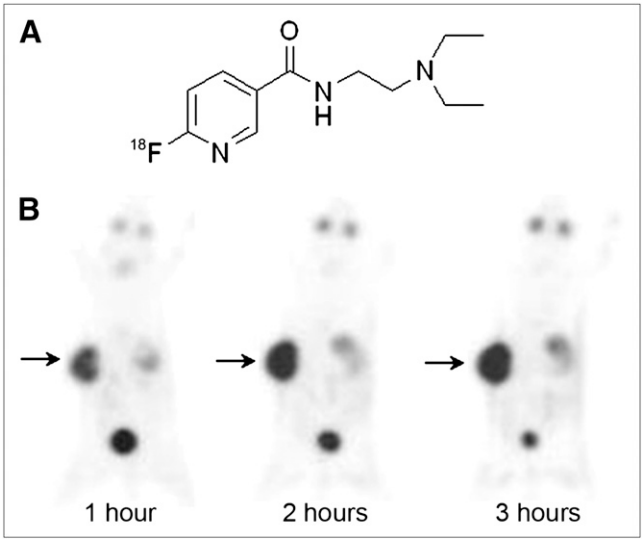

FIGURE 1. ^{18}F-MEL050 structure and PET images of B16-F0 melanoma–bearing mice. (A) ^{18}F-MEL050 chemical structure. (B) Maximum-intensity-projection whole-body PET images obtained at 1, 2, and 3 h after injection of 29.6 MBq of ^{18}F-MEL050 in C57BL/6 mouse bearing B16-F0 murine melanoma allograft. Tumor was implanted on right flank and is indicated with arrow on images.

The %ID/g of ^{18}F-MEL050 calculated from the PET images (Table 1) remained remarkably stable in the tumor over the 3-h time period. Thus, at 3 h the %ID/g in tumor reduced by only 6%, compared with the 1-h value (1 h, 9.6 ± 0.5, vs. 3 h, 9.0 ± 0.6), confirming the stability of the ^{18}F-MEL050 interaction with its target molecules. In the eyes and spleen, the %ID/g was also reasonably stable, with 60%−70% of the 1-h value remaining at 3 h. In contrast, the thyroid %ID/g of 2.2 ± 0.2 at 1 h had dropped by more than 70% (0.6 ± 0.04) between 1 and 3 h, rendering the thyroid signal barely detectable in the 3-h PET image (Fig. 1B).

^{18}F-MEL050 Melanin Specificity

The specificity of ^{18}F-MEL050 was examined by PET of tracer uptake at 1 h after injection in pigmented versus unpigmented melanoma models (Fig. 2). In the BALB/c nude mice, excellent tumor accumulation of ^{18}F-MEL050 was observed in the pigmented B16-F0 tumors, whereas no significant signal was present in A375 amelanotic melanoma xenografts. Furthermore, no radioactivity was retained in the eyes or spleen of the unpigmented mice. However, a modest signal was detectable in the thyroid in both C57BL/6 and BALB/c mice, confirming that specific binding to melanin is not involved in the low-level thyroid accumulation of ^{18}F-MEL050. To more closely examine the distribution of ^{18}F-MEL050 in tumor tissues, animals were sacrificed after PET and the tumors sectioned for high-resolution autoradiography (Fig. 2). In this analysis, it was clear that ^{18}F-MEL050 was specifically retained in cells across the entire section of the melanin-containing tumor, whereas there was virtually no signal in the unpigmented tumor section.

The close association of ^{18}F-MEL050 with melanin was further examined using the B16-BL6 metastatic melanoma model in which lung metastases arise approximately 2 wk after intravenous injection of melanoma cells. In this experiment, tumor-bearing mice were sacrificed 1 h after intravenous injection of approximately 30 MBq of ^{18}F-MEL050 and frozen sections of the lung tissue prepared. The sections were scanned by high-resolution autoradiography, and the isotopic images were compared with photographic images of the sections produced to localize the melanin-pigmented deposits (Fig. 3). These images

TABLE 1. Organ-to-Background Ratios (OBRs) and %ID/g of ^{18}F-MEL050 in Tissues of C57BL/6 Mice Bearing B16-F0 Tumor Allografts

	Tumor		Eyes		Spleen		Thyroid	
Time (h)	OBR	%ID/g	OBR	%ID/g	OBR	%ID/g	OBR	%ID/g
1	19.3 ± 1.9	9.6 ± 0.5	6.9 ± 1.1	2.9 ± 0.2	7.7 ± 0.9	3.7 ± 0.4	5.0 ± 0.9	2.2 ± 0.2
2	50.9 ± 6.9*	9.3 ± 0.7	14.9 ± 2.2†	2.2 ± 0.1†	13.7 ± 1.6*	2.9 ± 0.4	4.1 ± 0.4	0.9 ± 0.1†
3	54.3 ± 10.5*	9 ± 0.6	21 ± 2.5†	1.7 ± 0.04‡,§	16.8 ± 1.6*	2.6 ± 0.4	5 ± 0.9	0.6 ± 0.1†

1 h vs. 2 or 3 h: *$P < 0.05$; †$P < 0.01$; ‡$P < 0.001$, or 2 h vs. 3 h: §$P < 0.01$, as determined by *t* test.
Tissue uptake calculated from PET images after intravenous injection of 29.6 MBq of ^{18}F-MEL050 is expressed as mean ± SEM ($n = 6$).

highlight the strong concordance of the ^{18}F-MEL050 autoradiographic signals with the brown melanin–pigmented metastasis in the tissue photomicrographs.

Comparison of ^{18}F-MEL050 and ^{18}F-FDG for Melanoma Imaging

To assess the potential of ^{18}F-MEL050 as a complementary or competing PET tracer with ^{18}F-FDG for melanoma imaging, a further cohort of 6 B16-F0 tumor–bearing mice was scanned by ^{18}F-FDG PET at 2 h after tracer injection.

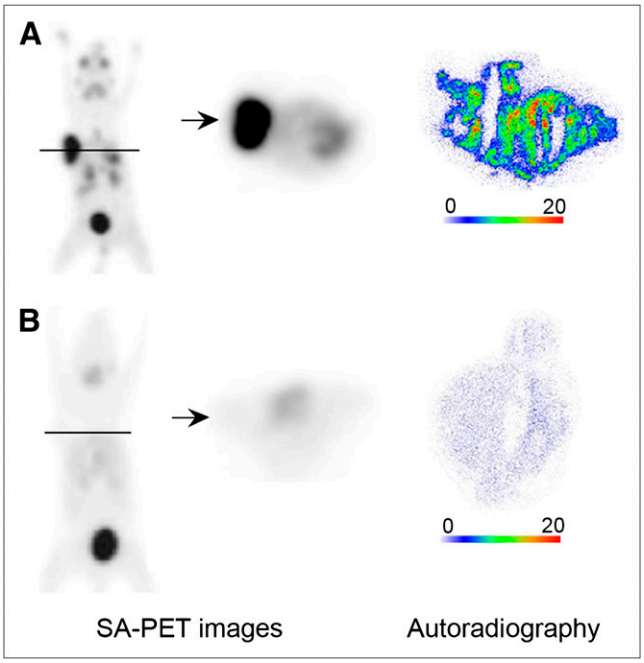

FIGURE 2. Specificity of ^{18}F-MEL050 for melanin. PET and autoradiographic images of C57BL/6 mouse bearing B16-F0 murine melanotic melanoma allograft (A) and BALB/c nude mouse bearing A375 human amelanotic melanoma xenograft (B). Coronal and transaxial PET images were obtained 1 h after injection of 22.2 MBq of ^{18}F-MEL050. Solid lines denote position of transaxial projection, and arrow marks site of tumor. Autoradiographic images of ^{18}F-MEL050 uptake are in frozen tumor sections. Scales indicate maximum pixel intensity expressed in counts/pixel. SA = small animal.

An example image from this experiment is shown in Figure 4. In this experiment, ^{18}F-FDG tumor uptake was compatible with uptake in other biologically aggressive cell lines, with a mean TBR of 5.8 ± 0.5. However, TBR for ^{18}F-MEL050 at 2 h was approximately 9-fold higher (50.9 ± 6.9). Although the overall background signal for ^{18}F-FDG in these mice was high, contributing somewhat to a reduced TBR, it is clear that ^{18}F-MEL050 PET yields a much clearer delineation of the melanoma deposits and, therefore, produces a vastly superior PET image for visualization of melanoma lesions.

^{18}F-MEL050 PET/CT of Metastatic Melanoma

To assess the potential of ^{18}F-MEL050 PET for the visualization of metastatic melanoma deposits, we used the B16-BL6 metastatic melanoma model in BALB/c nude mice. ^{18}F-MEL050 PET was performed 15 d after cell inoculation, when melanoma nodules in the lungs reach an approximate size of 1 mm as determined by autopsy in preliminary experiments (data not shown). Mice were then imaged on a clinical PET/CT scanner at 2 h after injection of ^{18}F-MEL050, and the presence of melanoma lesions in the lungs was clearly detected with ^{18}F-MEL050 PET (Fig. 5). After the PET/CT scan, the mice were sacrificed and the melanoma burden in the lungs assessed at necroscopy. From this examination, it was clear that the ^{18}F-MEL050 signal detected in the PET/CT images corresponded to the degree of melanoma invasion of the lung tissue.

DISCUSSION

In this preclinical imaging study, we report a new fluoronicotinamide analog specifically targeting primary and metastatic melanoma that is well suited to PET technology. Consistent with our previous pharmacokinetic study (*24*), ^{18}F-MEL050 exhibited favorable biologic properties, with excellent tumor retention and rapid clearance from nontarget tissues, primarily through renal clearance. These features allow the clear delineation of melanotic deposits as early as 1 h after tracer injection. ^{18}F-MEL050 tumor retention remains high for at least 3 h, suggesting a tight and stable binding interaction yielding an extremely high imaging contrast between tumor and nontarget tissues. Although the TBR of approximately 20:1 at 1 h would be

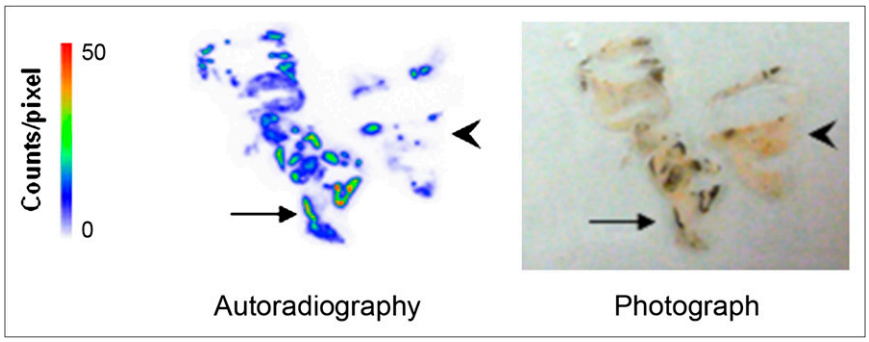

FIGURE 3. Correlation of ^{18}F-MEL050 uptake with melanoma deposits in B16 lung metastatic model. Shown are autoradiographic image and corresponding digital photomicrograph of frozen section through lung of C57BL/6 mouse bearing B16-BL6 metastatic lung lesions. Arrows and arrowheads indicate melanoma lesions and normal lung tissue, respectively.

sufficient for high-quality PET assessment of melanotic lesions in most instances, the plateau ^{18}F-MEL050 TBR of approximately 50:1 reached at 2 h represents a vast improvement over previously published results for other melanoma-specific PET probes. By comparison, clinical trials using ^{123}I-BZA showed that the best images were obtained 20 h after tracer injection, whereas the best results for ^{123}I-BZA$_2$ were seen at 4 h (*18,19,28*). However, these were planar imaging studies and no specific uptake values were reported; therefore, it was not possible to definitively compare the performance of these tracers with that of ^{18}F-MEL050. Nevertheless, the shorter half-life (110 min) and generally better availability of ^{18}F-fluoride than those of ^{123}I (half-life, 13.2 h)—and the technical advantages of PET with respect to resolution and quantitative potential, compared with γ-camera scintigraphy—suggest that ^{18}F-MEL050 will provide a much more efficient tracer for the clinical staging of melanoma. Furthermore, because of its rapid elimination through the urinary system, ^{18}F-MEL050 has the potential to improve the identification of melanomas localized to the liver and gastrointestinal tract for which anatomic imaging such as CT has limited sensitivity (*29*). Thus, ^{18}F-MEL050 PET has the potential to significantly improve treatment planning and identification of tumors suitable for surgical resection, the investigation of choice especially for patients with melanoma deposits in the bowel.

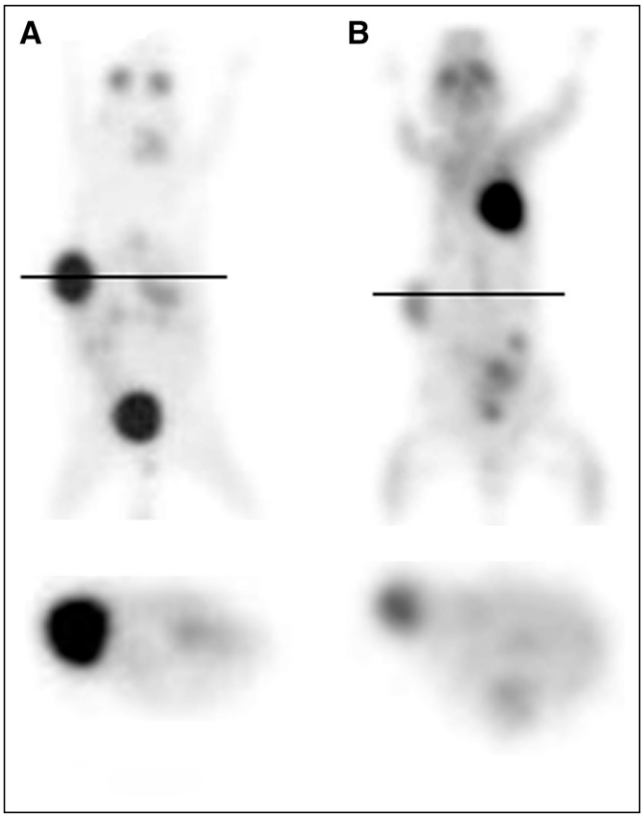

FIGURE 4. ^{18}F-MEL050 vs. ^{18}F-FDG PET analysis of murine melanoma. Coronal (top) and transaxial (bottom) projections of ^{18}F-MEL050 (A) and ^{18}F-FDG (B) PET images of C57BL/6 mice bearing B16-F0 tumors. Solid lines denote position of transaxial projections. PET images were obtained 2 h after injection of 20.13 MBq of ^{18}F-MEL050 and 17.7 MBq of ^{18}F-FDG.

In addition to the excellent uptake in the melanotic tumor deposits, a small amount of ^{18}F-MEL050 uptake was evident in the eyes and in some animals in the spleen, both melanin-pigmented tissues in C57BL/6 mice. This is likely due to the specific interaction of ^{18}F-MEL050 with melanin, because no ^{18}F-MEL050 is retained in these tissues in nonpigmented BALB/c nude mice or in A375 amelanotic tumor grafts. This result is in agreement with previously reported results for ^{123}I-MEL037, ^{125}I-BZA, and ^{125}I-BZA$_2$, all exhibiting high affinity for melanin (*22,30,31*). Moreover, despite a high ^{125}I-BZA$_2$ uptake in the eyes of C57BL/6 mice, clinical trials with ^{123}I-BZA$_2$ have shown no significant accumulation in human eyes and even demonstrated the feasibility of imaging ocular melanoma with melanin-specific probes (*19*). Thus, the uptake of tracers with melanin affinity in C57BL/6 mouse eyes is not necessarily predictive of the accumulation in human eyes.

A slight uptake of ^{18}F-MEL050 was also observed in the thyroid in C57BL/6 and in the unpigmented BALB/c nude mice. However, radioactivity decreases significantly over 3 h in thyroid tissue whereas tumor accumulation remains high, suggesting that thyroid accumulation does not involve a tight binding interaction such as that with melanin. In previous studies with iodinated BZA compounds, thyroid uptake has mainly been attributed to dehalogenation of the tracer (*32*). This is unlikely to be the explanation for the thyroid signal for ^{18}F-MEL050 because uptake of free ^{18}F-

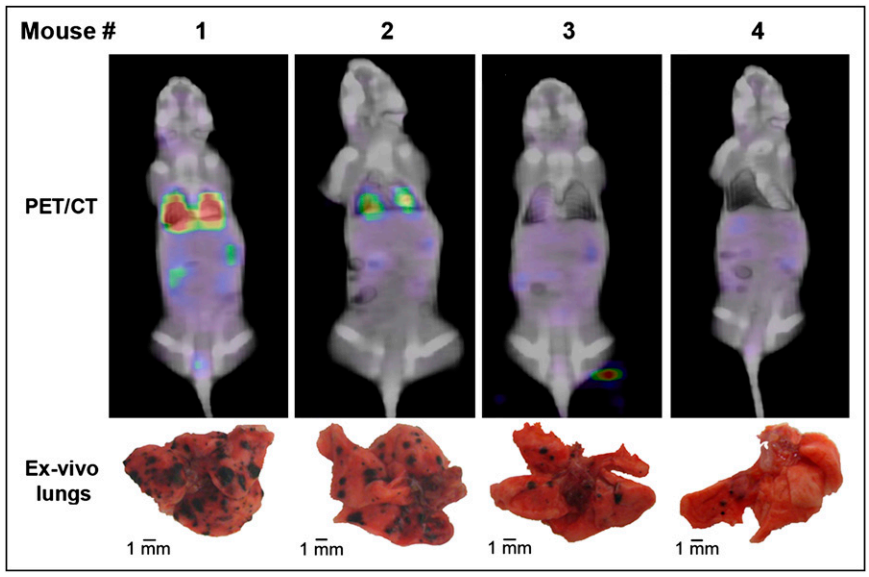

FIGURE 5. Analysis of lung metastatic disease by ^{18}F-MEL050 PET/CT and lesion counting. Superimposition of CT slices with correlative PET slices, with photographs of corresponding lung tissue specimens and lesion count, in 4 different mice exhibiting different levels of metastatic burden in lungs. PET/CT images were produced on human PET/CT scanner as described, approximately 1 h after injection of 18–20 MBq of ^{18}F-MEL050.

fluoride through iodine transporters on thyroid cells was excluded by giving the mice iodine before ^{18}F-MEL050 imaging. Also, the lack of bone uptake in any ^{18}F-MEL050 PET image supports our previous data (*24*), showing good in vivo stability of ^{18}F-MEL050 with respect to defluorination. Thus, the thyroid signal is most likely due to a weak nonspecific association of MEL050 with molecules in thyroid tissue, and as this association is transient it is unlikely to cause difficulties for melanoma imaging.

Currently, ^{18}F-FDG is considered to be the gold standard for clinical PET in melanoma. However, the high physiologic accumulation of ^{18}F-FDG in the heart, brain, and sometimes gastrointestinal tract presents problems for the detection of melanoma deposits in those locations. Further, ^{18}F-FDG imaging has limitations for the detection of smaller tumor deposits (*33*) and for use in settings of hyperglycemia (*34*) or inflammation (*35*). Consistent with this finding, several preclinical and clinical studies have reported the lack of sensitivity of ^{18}F-FDG PET for metastatic and uveal melanoma and the considerable improvement for the detection of melanoma lesions with melanoma-specific probes (*13,14*). We compared ^{18}F-MEL050 uptake with that of ^{18}F-FDG in a model of B16-F0 melanoma allograft. Despite good ^{18}F-FDG uptake in the B16-F0 tumors, tumor-to-body contrast was substantially lower than that of ^{18}F-MEL050, partially because of the somewhat higher background uptake of ^{18}F-FDG. Together with the high level of specificity for melanin-containing tumors, the superior contrast of ^{18}F-MEL050, compared with ^{18}F-FDG, suggests that ^{18}F-MEL050 in many instances will vastly improve the imaging of melanotic lesions by PET.

In our murine model of metastatic melanoma, high-resolution β-MicroImager autoradiography of lung tissue sections demonstrated the ability of ^{18}F-MEL050 to pinpoint small melanoma deposits in tissues. The β-MicroImager enabled the detection of radioactivity at the microregional level with a spatial resolution of 15 μm. This analysis highlights the tight specificity of ^{18}F-MEL050 for melanin-containing deposits and its strong potential to improve the detection of metastatic lesions in a clinical setting. To assess ^{18}F-MEL050 for the detection of melanoma metastases in a whole-animal model, we used a clinical PET/CT scanner to combine ^{18}F-MEL050 PET and anatomic data to improve the specific localization of lesions within tissues. The PET/CT images showed significant accumulation of ^{18}F-MEL050 in the lungs of mice bearing melanoma metastases. The level of ^{18}F-MEL050 signal in the PET/CT images reflected the tumor burden, with a strong link between the ^{18}F-MEL050 signal and the presence of melanoma deposits at necroscopy. The only background signals visible in these images were in the kidneys and bladder, representing residual tracer elimination through the urinary tract. Overall, these findings clearly demonstrated the outstanding ability of ^{18}F-MEL050 for noninvasive imaging of melanoma metastases in vivo.

A recent publication (*36*) describes the characterization of ^{18}F-FBZA, a melanin-binding benzamide with a chemical structure similar to that of ^{18}F-MEL050. ^{18}F-FBZA, however, had a lower tumor retention in the B16 melanoma tumors than did ^{18}F-MEL050 (^{18}F-FBZA %ID/g at 2 h = 5.94 ± 1.83 vs. 9.3 ± 0.7 for ^{18}F-MEL050). Further, ^{18}F-FBZA appeared to be cleared partially through the hepatobiliary system, with a %ID/g in the liver of 3.07 ± 0.8 at 2 h after tracer injection, whereas there was no evidence of hepatic clearance for ^{18}F-MEL050. In addition, the radiosynthesis time for ^{18}F-FBZA was 3 h, compared with 1 h for ^{18}F-MEL050. Thus, ^{18}F-MEL050 appeared to be a more likely candidate for translation as a clinical PET tracer for melanoma, especially for the identification of metastatic lesions in key organs such as the liver and bowel. In this context, there is increasing interest in the use of novel molecular targeted therapies directed at key genes known to be associated with malignant melanoma (*37*). The high specificity and sensitivity of ^{18}F-MEL050 for metastatic sites may aid the development of these novel therapies and

be of particular benefit for the evaluation of therapeutic efficacy.

CONCLUSION

We demonstrated in this study the feasibility of imaging murine melanoma allografts and metastatic deposits using ^{18}F-MEL050 PET. The favorable pharmacokinetic properties of this new fluoronicotinamide analog allowed the clear delineation of the tumor as early as 1 h after tracer injection, with almost complete background washout by 2 h. The high selectivity and affinity of ^{18}F-MEL050, compared with ^{18}F-FDG, for melanin offers the potential of simultaneously higher sensitivity and specificity for the identification of melanoma lesions and metastatic deposits using PET. Thus, our results suggest that ^{18}F-MEL050 PET has an excellent potential to improve the diagnosis and staging of melanoma.

ACKNOWLEDGMENTS

We gratefully acknowledge Laura Kirby, Susan Jackson, Rachael Walker, Kerry Ardley, Jiang Donghai, and Jeannette Valentan for their technical assistance and the radiochemistry team from Cyclotek (Aust) Pty Ltd. For financial support, we thank the Cooperative Research Centre for Biomedical Imaging Development Ltd. (CRCBID), established and supported under the Australian Government's Cooperative Research Centres program, and the Fondation de France.

REFERENCES

1. Balch CM, Soong SJ, Murad TM, Smith JW, Maddox WA, Durant JR. A multifactorial analysis of melanoma. IV. Prognostic factors in 200 melanoma patients with distant metastases (stage III). *J Clin Oncol.* 1983;1:126–134.
2. Balch CM, Soong SJ, Atkins MB, et al. An evidence-based staging system for cutaneous melanoma. *CA Cancer J Clin.* 2004;54:131–149.
3. Garbe C, Eigentler TK. Diagnosis and treatment of cutaneous melanoma: state of the art 2006. *Melanoma Res.* 2007;17:117–127.
4. Ollila DW, Caudle AS. Surgical management of distant metastases. *Surg Oncol Clin N Am.* 2006;15:385–398.
5. Krug B, Crott R, Lonneux M, Baurain JF, Pirson AS, Vander Borght T. Role of PET in the initial staging of cutaneous malignant melanoma: systematic review. *Radiology.* 2008;249:836–844.
6. Veit-Haibach P, Vogt FM, Jablonka R, et al. Diagnostic accuracy of contrast-enhanced FDG-PET/CT in primary staging of cutaneous malignant melanoma. *Eur J Nucl Med Mol Imaging.* 2009;36:910–918.
7. Wagner JD, Schauwecker D, Davidson D, et al. Inefficacy of F-18 fluorodeoxy-D-glucose-positron emission tomography scans for initial evaluation in early-stage cutaneous melanoma. *Cancer.* 2005;104:570–579.
8. Mittra E, Quon A. Positron emission tomography/computed tomography: the current technology and applications. *Radiol Clin North Am.* 2009;47:147–160.
9. Nabi HA, Zubeldia JM. Clinical applications of ^{18}F-FDG in oncology. *J Nucl Med Technol.* 2002;30:3–9.
10. Sobal G, Rodrigues M, Sinzinger H. Radioiodinated methylene blue: a promising agent for melanoma scintigraphy—labelling, stability and in vitro uptake by melanoma cells. *Anticancer Res.* 2008;28:3691–3696.
11. Beatovic S, Obradovic V, Latkovic Z, Jaksic E. Diagnosis and follow up of primary ocular melanoma by radioimmunoscintigraphy. *J BUON.* 2004;9:299–302.
12. Voss SD, Smith SV, DiBartolo N, et al. Positron emission tomography (PET) imaging of neuroblastoma and melanoma with ^{64}Cu-SarAr immunoconjugates. *Proc Natl Acad Sci USA.* 2007;104:17489–17493.
13. Kato K, Kubota T, Ikeda M, et al. Low efficacy of ^{18}F-FDG PET for detection of uveal malignant melanoma compared with ^{123}I-IMP SPECT. *J Nucl Med.* 2006;47:404–409.
14. Guo H, Shenoy N, Gershman BM, Yang J, Sklar LA, Miao Y. Metastatic melanoma imaging with an ^{111}In-labeled lactam bridge-cyclized α-melanocyte-stimulating hormone peptide. *Nucl Med Biol.* 2009;36:267–276.
15. Miao Y, Figueroa SD, Fisher DR, et al. ^{203}Pb-labeled α-melanocyte-stimulating hormone peptide as an imaging probe for melanoma detection. *J Nucl Med.* 2008;49:823–829.
16. Chezal JM, Papon J, Labarre P, et al. Evaluation of radiolabeled (hetero)aromatic analogues of *N*-(2-diethylaminoethyl)-4-iodobenzamide for imaging and targeted radionuclide therapy of melanoma. *J Med Chem.* 2008;51:3133–3144.
17. Pham TQ, Greguric I, Liu X, et al. Synthesis and evaluation of novel radioiodinated benzamides for malignant melanoma. *J Med Chem.* 2007;50:3561–3572.
18. Moins N, D'Incan M, Bonafous J, et al. ^{123}I-*N*-(2-diethylaminoethyl)-2-iodobenzamide: a potential imaging agent for cutaneous melanoma staging. *Eur J Nucl Med Mol Imaging.* 2002;29:1478–1484.
19. Sillaire-Houtmann I, Bonafous J, Veyre A, et al. Phase 2 clinical study of ^{123}I-*N*-(2-diethylaminoethyl)-2-iodobenzamide in the diagnostic of primary and metastatic ocular melanoma [in French]. *J Fr Ophtalmol.* 2004;27:34–39.
20. Bacin F, Michelot J, Bonafous J, et al. Clinical study of [^{123}I] *N*-(2-diethylaminoethyl)-4-iodobenzamide in the diagnosis of primary and metastatic ocular melanoma. *Acta Ophthalmol Scand.* 1998;76:56–61.
21. Larisch R, Schulte KW, Vosberg H, Ruzicka T, Muller-Gartner HW. Differential accumulation of iodine-123-iodobenzamide in melanotic and amelanotic melanoma metastases in vivo. *J Nucl Med.* 1998;39:996–1001.
22. Pham TQ, Berghofer P, Liu X, et al. Preparation and biologic evaluation of a novel radioiodinated benzylpiperazine, ^{123}I-MEL037, for malignant melanoma. *J Nucl Med.* 2007;48:1348–1356.
23. Garg S, Kothari K, Thopate SR, Doke AK, Garg PK. Design, synthesis, and preliminary in vitro and in vivo evaluation of *N*-(2-diethylaminoethyl)-4-[^{18}F]fluorobenzamide ([^{18}F]-DAFBA): a novel potential PET probe to image melanoma tumors. *Bioconjug Chem.* 2009;20:583–590.
24. Greguric I, Taylor SR, Denoyer D, et al. Discovery of [^{18}F]*N*-(2-(diethylamino)ethyl)-6-fluoronicotinamide: a melanoma positron emission tomography imaging radiotracer with high tumor to body contrast ratio and rapid renal clearance. *J Med Chem.* 2009;52:5299–5302.
25. Huisman MC, Reder S, Weber AW, Ziegler SI, Schwaiger M. Performance evaluation of the Philips MOSAIC small animal PET scanner. *Eur J Nucl Med Mol Imaging.* 2007;34:532–540.
26. Chiang S, Cardi C, Matej S, et al. Clinical validation of fully 3-D versus 2.5-D RAMLA reconstruction on the Philips-ADAC CPET PET scanner. *Nucl Med Commun.* 2004;25:1103–1107.
27. Tanaka E, Kudo H. Subset-dependent relaxation in block-iterative algorithms for image reconstruction in emission tomography. *Phys Med Biol.* 2003;48:1405–1422.
28. Michelot JM, Moreau MF, Veyre AJ, et al. Phase II scintigraphic clinical trial of malignant melanoma and metastases with iodine-123-*N*-(2-diethylaminoethyl 4-iodobenzamide). *J Nucl Med.* 1993;34:1260–1266.
29. Lens M, Bataille V, Krivokapic Z. Melanoma of the small intestine. *Lancet Oncol.* 2009;10:516–521.
30. Mansard S, Papon J, Moreau MF, et al. Uptake in melanoma cells of *N*-(2-diethylaminoethyl)-2-iodobenzamide (BZA_2), an imaging agent for melanoma staging: relation to pigmentation. *Nucl Med Biol.* 2005;32:451–458.
31. Chehade F, De Labriolle-Vaylet C, Michelot J, et al. Distribution of I-BZA (*N*-2-diethylaminoethyl-4-iodobenzamide) in grafted melanoma and normal skin: a study by secondary ion mass spectroscopy. *Cell Mol Biol (Noisy-le-grand).* 2001;47:529–534.
32. Verhoeff NP, Sokole EB, Stabin M, et al. Dosimetry of iodine-123 iodobenzamide in healthy volunteers. *Eur J Nucl Med.* 1993;20:747–752.
33. Ho Shon IA, Chung DK, Saw RP, Thompson JF. Imaging in cutaneous melanoma. *Nucl Med Commun.* 2008;29:847–876.
34. Li TR, Tian JH, Wang H, Chen ZQ, Zhao CL. Pitfalls in positron emission tomography/computed tomography imaging: causes and their classifications. *Chin Med Sci J.* 2009;24:12–19.
35. Takahashi H, Ukawa K, Ohkawa N, et al. Significance of ^{18}F-2-deoxy-2-fluoro-glucose accumulation in the stomach on positron emission tomography. *Ann Nucl Med.* 2009;23:391–397.
36. Ren G, Miao Z, Liu H, et al. Melanin-targeted preclinical PET imaging of melanoma metastasis. *J Nucl Med.* 2009;50:1692–1699.
37. Haluska F, Pemberton T, Ibrahim N, Kalinsky K. The RTK/RAS/BRAF/PI3K pathways in melanoma: biology, small molecule inhibitors, and potential applications. *Semin Oncol.* 2007;34:546–554.